

Transient Buoyancy- Driven Laminar Convection in an Inclined Three- Dimensional Trapezoidal Enclosure.

Ahmed Kadhim Hussein

Department of Mechanical Engineering
University of Babylon

College of Engineering

E-mail :ahmedkadhim7474@gmail.com

Kolsi Lioua

Department of Energy Engineering
University Monastir , Tunisia

College of Engineering

Hussain H. Al-Kayiem

Department of Mechanical Engineering
University of Teknologi PETRONAS , 31750

Tronoh , Perak , Malaysia

College of Engineering

Abstract- Numerical analysis of transient laminar three-dimensional buoyancy-driven convection in an inclined three-dimensional trapezoidal air-filled enclosure was investigated in this paper. The right and left sidewalls of the enclosure are kept at constant cold temperatures. The bottom wall is maintained at a constant hot temperature , while the top wall is considered adiabatic. Numerical investigation is performed for Rayleigh numbers varied as $10^3 \leq Ra \leq 10^5$, while the trapezoidal enclosure inclination angle is varied as $0^\circ \leq \Phi \leq 180^\circ$. Prandtl number is considered constant at $Pr = 0.71$. Flow and thermal fields are presented in both two and three-dimensional pattern. Also, both local and average Nusselt numbers are calculated and discussed. The results show that when the Rayleigh number increases, the flow patterns are changed especially in three-dimensional results and the flow circulation increases. The minimum average Nusselt number inside the trapezoidal cavity corresponds to the highest inclination angle [i.e., $\Phi = 180^\circ$]. While, the average Nusselt number reaches its maximum value at $\Phi = 30^\circ$. Moreover, when the Rayleigh number increases the average Nusselt number increases as expected.

Key words: Transient convection , Trapezoidal enclosure , 3D , Laminar flow , Inclined enclosure.

I. Introduction

Buoyancy-driven or natural convection in enclosures of various geometries has taken considerable attention in the past few decades due to its many significant applications such as electronic components cooling , heating and preservation of canned foods , nuclear reactors and heat exchangers [1-2]. The study of buoyancy-driven in a trapezoidal enclosure is difficult than the classical square or rectangular cavities due to the presence of inclined walls. This complex geometry needs an accurate effect in grid generation and code construction. However, many studies were available on buoyancy-driven convection concerned trapezoidal enclosure. Lam et al. [3] performed an experimental and numerical studies of natural convection in trapezoidal cavities composed of two vertical insulated sidewalls, an inclined cold top wall and a horizontal hot bottom wall. The obtained results illustrated that the onset of natural convection in a trapezoidal cavity occurred at lower Ra as the angle of inclination was increased from zero. Kumar [4] studied experimentally the natural convection in a trapezoidal enclosure of a box-type solar cooker .He concluded that the major advantage of this geometry was the absorption of a higher fraction of incident solar radiation falling on the aperture at larger incidence

angles. Basak et al. [5] investigated numerically the natural convection in trapezoidal enclosures for uniformly heated bottom wall and linearly heated vertical wall(s) in presence of insulated top wall. Average Nusselt number plots showed higher heat transfer rates for ($\phi = 0^\circ$ with the vertical) and the overall heat transfer rates at the bottom wall was larger for the linearly heated left wall and cooled right wall. Lasfer et al. [6] investigated numerically the steady natural convection of air flow in a two-dimensional side-heated trapezoidal room. The results indicated a great dependence of the flow fields and the heat transfer on inclination angle, aspect ratio and Rayleigh number. Basak et al. [7] studied numerically the natural convection flow in closed trapezoidal enclosures with linearly heated sidewalls and linearly heated left wall and cold right wall. In both cases the bottom wall was uniformly heated while top wall was insulated. They concluded that, overall heat transfer rates were larger for square cavity ($\phi = 90^\circ$ with the horizontal) compared to other angles ($\phi = 45^\circ$ and 60°). Sahoo et al. [8] investigated numerically the heat loss due to radiation and steady laminar natural convection flow in a trapezoidal cavity having eight absorber tubes for a Linear Fresnel Reflector (LFR) solar thermal system with uniformly heated tubes and adiabatic top and side walls. They suggested a correlation between the total average Nusselt number and its influencing parameters for the proposed cavity. Natarajan et al. [9] performed a numerical study of combined natural convection and surface radiation in a solar trapezoidal cavity absorber for Compact Linear Fresnel Reflector (CLFR). The results were presented in terms of Nusselt number correlation to show the effect of these parameters on combined natural convection and surface radiation heat loss. Mustafa and Ghani [10] investigated numerically the natural convection in a trapezoidal enclosure with partial heating from below and symmetrical cooling from the sides. They concluded that the average Nusselt number increased with the increase of the source length. Da Silva et al. [11] investigated numerically the natural convection in trapezoidal cavities, especially those with two internal baffles in conjunction with an insulated floor, inclined top surface, and isothermal left-heated and right-cooled vertical walls. A correlation for the average Nusselt number in terms of Prandtl and Rayleigh numbers, and the inclination of the upper surface of the cavity was proposed for each baffle height investigated. Tracy and Crunkleton [12] studied numerically the natural convective flow oscillations in isosceles trapezoidal enclosures for three vertex angles with the horizontal (22° , 45° and 67°). They concluded that as

the base angle was decreased, various disturbances were superimposed over flow oscillations.

From the other side, the three-dimensional natural convection in cavities was investigated by many researchers. **Hiller et al. [13]** investigated experimentally and numerically the transient natural convection in a cube-shaped cavity with two isothermal copper walls kept at a prescribed temperature. They observed that in the vicinity of the sidewalls, the temperature gradients were largest and isotherms were nearly vertical. **Frederick [14]** studied numerically the natural convection in a cubical enclosure with two equal active sectors on one vertical wall over a wide range of Rayleigh number. He concluded that Nusselt numbers exceeded the ones for a side heated cavity at low Rayleigh number. **Frederick and Moraga [15]** numerically investigated the three-dimensional natural convection of air in a cubical enclosure with a fin on the hot wall for Rayleigh numbers of (10^3 - 10^6). The fin with a thickness of (1/10) of the cavity side was placed horizontally on the hot wall. The solid to fluid thermal conductivity ratio (R_k) and the fin width were varied. It was concluded that for $10^5 \leq Ra \leq 10^6$, a fin of partial width was more effective in promoting heat transfer than a fin of full width. **Oosthuizen et al. [16]** numerically studied the three-dimensional natural convective flow in a rectangular enclosure with vertical sidewalls and horizontal top and bottom surfaces. A heated isothermal rectangular element was mounted on the centre of one vertical wall of the enclosure while the horizontal top surface of it cooled to a uniform temperature. All other enclosure surfaces were adiabatic. They concluded that the relative change in mean Nusselt number with decreasing dimensionless width of plate increased as the Rayleigh number decreased. **Bocu and Altac [17]** studied numerically the laminar natural convection heat transfer in 3D rectangular air filled enclosures, with pins attached to the active wall. Two cases of rectangular enclosures were considered ($H/L = 1$ and $H/L = 2$). The results explained that the Nusselt number ratio with respect to the enclosure without pins increased with pin length, pin number and for tall enclosures. Another works related with the three-dimensional natural convection in a three-dimensional cavity can be found in [18-20]. The above literature review indicated that the published papers related with the analysis of buoyancy-driven was available in two-dimensional trapezoidal enclosures only. According to our knowledge, the investigation of this problem in a three-dimensional trapezoidal inclined enclosure has not been considered yet in the literature. Therefore, this problem is studied in the present paper.

2. Mathematical model and numerical solution

The buoyancy-driven problem inside an inclined three-dimensional trapezoidal enclosure of height (H), length (L) and depth (W) filled with air ($Pr = 0.71$) is investigated in the present work as shown in **Fig.1**. The right and left sidewalls of a trapezoidal enclosure are kept at isothermal cold temperatures (T_c) and inclined at an angle of 30° . The top wall is adiabatic while bottom one is subjected to an isothermal hot temperature (T_h). The flow field inside the enclosure is considered three-dimensional, Newtonian, transient, incompressible and laminar. The Rayleigh number is varied as $10^3 \leq Ra \leq 10^5$, while the trapezoidal

enclosure inclination angle is varied as $0^\circ \leq \Phi \leq 180^\circ$. The fluid inside the enclosure is assumed to have a constant thermo-physical properties and Boussinesq approximation is used to model the density variation. To start the numerical approach, the vorticity-vector potential formalism ($\vec{\omega} - \vec{\omega}$) is considered in the present work which allowed in a three-dimensional geometry, and elimination of the pressure gradient term. Vector potential and the vorticity are defined respectively by the following two equations:

$$\vec{\omega}' = \vec{\nabla} \times \vec{V}' \quad \text{and} \quad \vec{V}' = \vec{\nabla} \times \vec{\psi}' \tag{1}$$

The construction of these equations are described in more details in **Ghachem et al. [21]**. The dimensionless governing equations can be written as follows [21]:

$$-\vec{\omega} = \nabla^2 \vec{\psi} \tag{2}$$

$$\frac{\partial \vec{\omega}}{\partial t} + (\vec{V} \cdot \nabla) \vec{\omega} - (\vec{\omega} \cdot \nabla) \vec{V} = \Delta \vec{\omega} + Ra.Pr. \begin{bmatrix} \frac{\partial T}{\partial z} \cos \Phi \\ -\frac{\partial T}{\partial z} \sin \Phi \\ -\frac{\partial T}{\partial x} \cos \Phi + \frac{\partial T}{\partial y} \sin \Phi \end{bmatrix} \tag{3}$$

$$\frac{\partial T}{\partial t} + \vec{V} \cdot \nabla T = \nabla^2 T \tag{4}$$

$$\text{where} \quad Pr = \frac{\nu}{\alpha} \quad \text{and} \quad Ra = \frac{g\beta(T_h - T_c)L^3}{\nu\alpha}$$

The initial conditions for the present problem are given as follows:

$$\text{at } t=0 \quad V_x = V_y = V_z = 0$$

The boundary conditions are given as follows:

Temperature:

$$T = 1 \quad \text{at } y=0 \text{ [at bottom wall]}, \quad T = 0 \quad \text{at the inclined sidewalls}$$

$$\frac{\partial T}{\partial n} = 0 \quad \text{on all other walls (adiabatic)}$$

Vorticity:

$$\omega_x = 0, \quad \omega_y = -\frac{\partial V_z}{\partial x}, \quad \omega_z = \frac{\partial V_y}{\partial x} \quad \text{at } x=0 \text{ and } 1$$

$$\omega_x = \frac{\partial V_z}{\partial y}, \quad \omega_y = 0, \quad \omega_z = -\frac{\partial V_x}{\partial y} \quad \text{at inclined sidewalls}$$

$$\omega_x = -\frac{\partial V_y}{\partial z}, \quad \omega_y = \frac{\partial V_x}{\partial z}, \quad \omega_z = 0 \quad \text{at } z=0 \text{ and } 1$$

Vector potential:

$$\frac{\partial \Psi_x}{\partial x} = \Psi_y = \Psi_z = 0 \quad \text{at } x=0 \text{ and } 1$$

$$\Psi_x = \frac{\partial \Psi_y}{\partial y} = \Psi_z = 0 \quad \text{at inclined sidewalls}$$

$$\Psi_x = \Psi_y = \frac{\partial \Psi_z}{\partial z} = 0 \text{ at } z = 0 \text{ and } 1$$

Velocity :

$$V_x = V_y = V_z = 0 \text{ on all 3D trapezoidal enclosure walls}$$

The local and average Nusselt numbers are given by :

$$Nu = \frac{\partial T}{\partial x} \Big|_{y=0} \quad \text{and} \quad Nu_{av} = \int_0^1 \int_0^1 Nu \cdot dy \cdot dz \quad (5)$$

The mathematical model described above was written by a FORTRAN program. The finite volume method is used to discretize governing equations [(2)-(4)]. The grids are considered uniform in all directions with clustering nodes on boundaries. The successive relaxation iteration scheme is used to solve the resulting non-linear algebraic equations. The time step (10^{-4}) and spatial mesh ($51 \times 151 \times 76$) are utilized to carry out all the numerical tests. The solution is considered acceptable when the following convergence criterion is satisfied for each step of time :

$$\sum_i^{1,2,3} \frac{\max |\psi_i^n - \psi_i^{n-1}|}{\max |\psi_i^n|} + \max |T_i^n - T_i^{n-1}| \leq 10^{-4} \quad (6)$$

In order to verify the accuracy of the present program. The problem of natural convection flow in a trapezoidal enclosure considered by **Basak et al. [22]** is resolved by the present program and a good agreement is obtained as shown in Table 1.

3. Results and discussion

The transient laminar buoyancy-driven convection in an inclined 3D trapezoidal air-filled enclosure is investigated numerically in this work. The effect of Rayleigh number (Ra) and cavity inclination angle (Φ) on the flow and thermal fields have been performed.

3.1 Effect of Rayleigh number on thermal and flow fields.

Figure 2 illustrates is surfaces of temperature around the all geometry (left) and isotherms along the mid-section ($Z = 0.5$) (right) in the three-dimensional trapezoidal cavity ($\Phi = 0^\circ$) for various values of Rayleigh number ((a) $Ra = 10^3$, (b) $Ra = 10^4$ and (c) $Ra = 10^5$). When the Rayleigh number is low ($Ra = 10^3$) or when the effect of natural convection is slight , the isotherms are smooth and straight lines. This behavior is due to flow weakness when the Rayleigh number is low ($Ra = 10^3$). It can be seen from **Fig.2** , that isotherms emanate from the lower wall (or base) where the heat source exists and end on cold right and left sidewalls , indicating the heat flow path. Heat conduction is the dominant mechanism of heat transfer inside the trapezoidal cavity in this case. But , as the Rayleigh number increases to ($Ra = 10^4$ and $Ra = 10^5$) , buoyancy force dominates over viscous force leading to increase the natural convection effect. Therefore, the shape of isotherms begins to deviate sharply from uniform one encountered in the case where ($Ra = 10^3$). This is due to the strong circulation occurs when the Rayleigh number is high. The concentration of isotherms adjacent the lower wall increases as the Rayleigh

number increases illustrating high amount of heat and large temperature gradient adjacent the lower wall of the cubical trapezoidal cavity. Therefore, a thermal boundary layer is constructed at this region and can be observed especially when ($Ra = 10^5$). Heat convection is the dominant mechanism of heat transfer in this case. Therefore , it can be concluded that there is a clear conversion in isotherms pattern from uniform smooth shape to a high confuse one as the Rayleigh number increases. This behavior gives a clear approval of natural convection effect on the thermal field inside the cubical trapezoidal cavity. **Figure 3** presents the trajectory of particles around the whole geometry (left) and streamlines along the mid-section ($Z = 0.5$) (right) in the cubical trapezoidal cavity ($\Phi = 0^\circ$) for various values of Rayleigh number ((a) $Ra = 10^3$, (b) $Ra = 10^4$ and (c) $Ra = 10^5$). According to the natural convection effect, the flow field begins to move from the hot lower wall until it arrives to the insulated upper wall. Then , it changes its direction and moves towards the cold right and left sidewalls after passing secondly adjacent the hot lower wall. This cyclic motion of the flow field generates the re-circulating vortices which occupy all span of the trapezoidal cavity as can be seen in **Fig.3**. It can be noticed that the air stream which moves upward adjacent the hot lower wall separates into two re-circulating vortices as indicated in 3D results. This flow behavior can be seen for all the considered values of Rayleigh number , but there is a difference in the shape of vortices related with the value of Rayleigh number. In the case of low Rayleigh number ($Ra = 10^3$) , the effect of buoyancy force [which is generated due to the temperature difference] is slight and the flow circulation is uniform . Therefore , the convection effect is weak. Now , when the Rayleigh number increases to ($Ra = 10^4$ and $Ra = 10^5$) or when the effect of buoyancy force is significant, the frictional resistance to the fluid motion diminishes gradually. Therefore, the flow circulation becomes less uniform. It can be observed that, the strict uniform pattern of re-circulating vortices encountered at ($Ra = 10^3$) is broken due to the strong effect of natural convection inside the cubical trapezoidal cavity. While , a weak fluid motion is noticed at the edges of the cubical cavity for all the considered range of Rayleigh number. Moreover , it can be seen also that the difference between the two-dimensional and three-dimensional results becomes clear as Rayleigh number increases from ($Ra = 10^3$) to ($Ra = 10^5$).

3.2 Effect of Rayleigh number on local and average Nusselt numbers.

Figure 4 demonstrates x-z profiles of local Nusselt numbers (Nu_{Loc}) at the hot lower wall in the trapezoidal cavity ($\Phi = 0^\circ$) for various values of Rayleigh number ((a) $Ra = 10^3$, (b) $Ra = 10^4$ and (c) $Ra = 10^5$). These profiles reveal that the local Nusselt number is linear at low Rayleigh number ($Ra = 10^3$). This indicates that the heat is transferred inside the trapezoidal cavity by pure conduction. But , as the Rayleigh number increases to ($Ra = 10^4$ and $Ra = 10^5$) , local Nusselt number profiles start to change its shape indicating the onset of natural convection. However , at ($Ra = 10^4$) , the local Nusselt profiles are still in the transition process from conduction mode to a fully convection one. Moreover, it is interesting to observe high values of the local Nusselt number adjacent the cavity hot lower wall due to the existence of heat source at this place. **Figure 5**

illustrates the effect of Rayleigh number on the average Nusselt number (Nu_{av}) at ($\Phi = 0^\circ$). The average Nusselt number is a measure of the heat transfer rate inside the cubical trapezoidal cavity. It can be seen as expected, that the average Nusselt number increases as the Rayleigh number increases. This is because the natural convection and flow circulation are enhanced when the Rayleigh number increases. Therefore, the highest average Nusselt number corresponds to the highest Rayleigh number and vice versa. The reason of this behavior is due to the increase in the temperature gradient when the Rayleigh number increases. This increasing leads to the average Nusselt number increasing.

3.3 Effect of inclination angle on thermal and flow fields.

Fig.6 shows the isosurfaces of temperature around the whole geometry (upper) and isotherms a long the mid-section [$Z=0$] (lower) in the trapezoidal cavity at ($Ra = 10^5$) and various values of inclination angles (a) $\Phi = 0^\circ$; (b) $\Phi = 30^\circ$; (c) $\Phi = 60^\circ$; (d) $\Phi = 90^\circ$; (e) $\Phi = 120^\circ$; (f) $\Phi = 150^\circ$ and (g) $\Phi = 180^\circ$. For horizontal trapezoidal cavity ($\Phi = 0^\circ$), the thermal field is governed by the Rayleigh number effect only which is explained previously in **Fig.2**. Since, the value of the selected Rayleigh number is high [i.e., $Ra = 10^5$], therefore the natural convection effect is strong which causes to make the thermal field represented by isotherms and isosurfaces of temperature are non-uniform. Now, when the cavity inclination angle increases to $\Phi = 30^\circ$ and 60° respectively, the effect of natural convection decreases slightly and the disturbance in the isotherms becomes less than the corresponding one which is observed at $\Phi = 0^\circ$. Furthermore, the thermal boundary layers adjacent the hot lower wall become less thicker than that observed at ($\Phi = 0^\circ$). For vertical cubical trapezoidal cavity ($\Phi = 90^\circ$), the thermal field becomes somewhat uniform indicating the beginning of the conduction mode of the heat transfer inside the cavity. But, when the cavity inclination angle increases to $\Phi = 120^\circ$, 150° and 180° respectively, the pattern of isotherms will change completely especially at $\Phi = 180^\circ$. The isotherms are uniformly space distributed inside the cavity implying the absence of convection. **Fig.7** displays the trajectory of particles around the all geometry (upper) and streamlines a long the mid-section ($Z=0$) (lower) in the trapezoidal cavity at ($Ra = 10^5$) and various values of inclination angle. Results demonstrate that the inclination angle has a significant role on the flow pattern. When the inclination angle is $\Phi = 0^\circ$ and 30° , the flow field inside the cavity can be represented by two symmetrical re-circulating vortices. The effect of buoyancy force in this case is high. But, when the cavity inclination angle increases to $\Phi = 60^\circ$ and 90° , the flow field inside the cavity is represented by a single large re-circulating vortex. As, the cavity inclination angle increases to $\Phi = 120^\circ$, 150° and 180° respectively, the flow field inside the cavity is characterized again by two asymmetrical re-circulating vortices. The effect of natural convection in this case begins to decrease gradually as the cavity inclination angle increases.

3.4 Effect of inclination angle on average Nusselt numbers.

Fig.8 illustrates the relationship between the average Nusselt numbers in the trapezoidal cavity and Rayleigh number for various values of inclination angle. It is found that the average Nusselt number reaches its maximum value at $\Phi = 30^\circ$. While, the minimum value of the average Nusselt number is reached at $\Phi = 180^\circ$. The reason of this behavior because the bottom hot wall becomes in the upper position and as a result, the convection effect becomes insignificant. This increasing reduces the temperature gradient and causes to drop the average Nusselt number values. **Fig.9** depicts the relationship between the average Nusselt numbers in the cubical trapezoidal cavity and inclination angle for various values of Rayleigh number. It can be seen that the average Nusselt number is an increasing function of Rayleigh number due to the significant increase in the convection effect as expected. The results show also that when the inclination angle in the range $0^\circ \leq \Phi \leq 90^\circ$, the effect of Rayleigh number is greater than its effect when the inclination angle in the range $120^\circ \leq \Phi \leq 180^\circ$. The reason of this behavior is explained previously.

4. Conclusions

Numerical analysis of transient laminar three-dimensional buoyancy-driven convection in an inclined three-dimensional trapezoidal air-filled enclosure was investigated in this paper. The results indicated that the minimum average Nusselt number inside the enclosure corresponds to the highest inclination angle ($\Phi = 180^\circ$) while, the average Nusselt number reaches its maximum value at ($\Phi = 30^\circ$). The difference between the two-dimensional and three-dimensional flow pattern results becomes clear as the Rayleigh number increases. Also, the flow pattern inside the enclosure consists of four spiral re-circulating vortices which cover all the span of it. The local Nusselt number distribution is almost parallel to the horizontal upper and lower cavity walls. Different flow patterns can be seen inside the cubical trapezoidal cavity as the inclination angle increases from $\Phi = 0^\circ$ to $\Phi = 180^\circ$. This gives an important indication that the flow field inside the cavity are significantly affected by the inclination angle.

5. References

- [1] Turan, O., Poole, R. and Chakraborty, N. Aspect ratio effects in laminar natural convection of Bingham fluids in rectangular enclosures with differentially heated side walls, *Journal of Non-Newtonian Fluid Mechanics*, Vol.166, 2011, pp : 208-230.
- [2] Turan, O., Poole, R. and Chakraborty, N. Influences of boundary conditions on laminar natural convection in rectangular enclosures with differentially heated side walls, *International Journal of Heat and Fluid Flow*, Vol. 33, 2012, pp : 131-146.
- [3] Lam, S., Gani, R. and Simons, J. Experimental and numerical studies of natural convection in trapezoidal cavities, *ASME Journal of Heat Transfer*, Vol. 111, 1989, pp: 372-377.

- [4] Kumar, S. Natural convective heat transfer in trapezoidal enclosure of box-type solar cooker , *Renewable Energy*, Vol. 29, 2004, pp : 211-222.
- [5] Basak, T., Roy, S. , Singh , A. and Pandey, B. Natural convection flow simulation for various angles in a trapezoidal enclosure with linearly heated side wall(s) , *International Journal of Heat and Mass Transfer*, Vol. 52, 2009, pp : 4413-4425.
- [6] Lasfer, K., Bouzaiane, M. and Lili , T. Numerical study of laminar natural convection in a side-heated trapezoidal cavity at various inclined heated sidewalls , *Heat Transfer Engineering* ,Vol.31, No.5, 2010, pp : 362-373.
- [7] Basak, T., Ramakrishna , D. , Roy, S. , Matta , A. and Pop, I. A comprehensive heatline based approach for natural convection flows in trapezoidal enclosures: Effect of various walls heating , *International Journal of Thermal Sciences*, Vol. 50, 2011, pp : 1385-1404.
- [8] Sahoo, S., Singh, S. and Banerjee,R. Analysis of heat losses from a trapezoidal cavity used for Linear Fresnel Reflector system , *Solar Energy* ,Vol. 86 , 2012, pp: 1313-1322.
- [9] Natarajan, S. , Reddy , K. and Mallick , T. Heat loss characteristics of trapezoidal cavity receiver for solar linear concentrating system , *Applied Energy* , Vol. 93, 2012 , pp : 523-531.
- [10] Mustafa, A. and Ghani , I. Natural convection in trapezoidal enclosure heated partially from below , *Al-Khwarizmi Engineering Journal* , Vol.8, No.1 2012 , pp : 76-85.
- [11] Da silva, A., Fontana , E. , Mariani , V. and Marcondes, F. Numerical investigation of several physical and geometric parameters in the natural convection into trapezoidal cavities , *International Journal of Heat and Mass Transfer* , Vol. 55 , 2012, pp: 6808-6818.
- [12] Tracy, N. and Crunkleton, D. Oscillatory natural convection in trapezoidal enclosures , *International Journal of Heat and Mass Transfer* ,Vol. 55, 2012, pp : 4498-4510.
- [13] Hiller , W., Koch,S. , Kowalewski ,T. and Stella , F. Onset of natural convection in a cube , *International Journal of Heat and Mass Transfer*, Vol. 13 , 1993, pp: 3251-3263.
- [14] Frederick , R. Natural convection heat transfer in a cubical enclosure with two active sectors on one vertical wall , *International Communications in Heat and Mass Transfer* , Vol. 24 , No.4 , 1997, pp: 507-520.
- [15] Frederick , R. and Moraga , S. Three-dimensional natural convection in finned cubical enclosures , *International Journal of Heat and Fluid Flow* , Vol. 28 , 2007, pp: 289-298.
- [16] Oosthuizen, P., Kalendar, A. and Simko , T. Three-dimensional natural convective flow in a rectangular enclosure with a rectangular heated section on one vertical wall and a cooled horizontal upper wall , *5th European Thermal-Sciences Conference*, 2008, Netherlands , pp: 1-8.
- [17] Bocu, Z. and Altac ,Z. Laminar natural convection heat transfer and air flow in three-dimensional rectangular enclosures with pin arrays attached to hot wall , *Applied Thermal Engineering*, Vol. 31, 2011, pp: 3189-3195.
- [18] Da silva, A. and Gosselin, L. On the thermal performance of an internally finned 3D cubic enclosure in natural convection , *International Journal of Thermal Sciences*,Vol. 44, 2005, pp : 540-546.
- [19] Bennett, B. and Hsueh, J. Natural convection in a cubic cavity : implicit numerical solution of two benchmark problems , *Numerical Heat Transfer, Part A* ,Vol.50, 2006, pp : 99-107.
- [20] Lo, D. and Leu, S. DQ analysis of 3D natural convection in an inclined cavity using an velocity-vorticity formulation , *Proceedings of World Academy of Science, Engineering and Technology* ,Vol. 36, 2008, pp : 370–375.
- [21] Ghachem, K. , Kolsi , L. , Mâatki , C. , Hussein , A. and Borjini, M. Numerical simulation of three-dimensional double diffusive free convection flow and irreversibility studies in a solar distiller , *International Communications in Heat and Mass Transfer*, Vol.39, 2012, pp: 869-876.
- [22] Basak,T., Roy, S., Singh,A. and Pop,I. Finite element simulation of natural convection flow in a trapezoidal enclosure filled with porous medium due to uniform and non-uniform heating, *International Journal of Heat and Mass Transfer* ,Vol. 52, 2009, pp : 70–78.

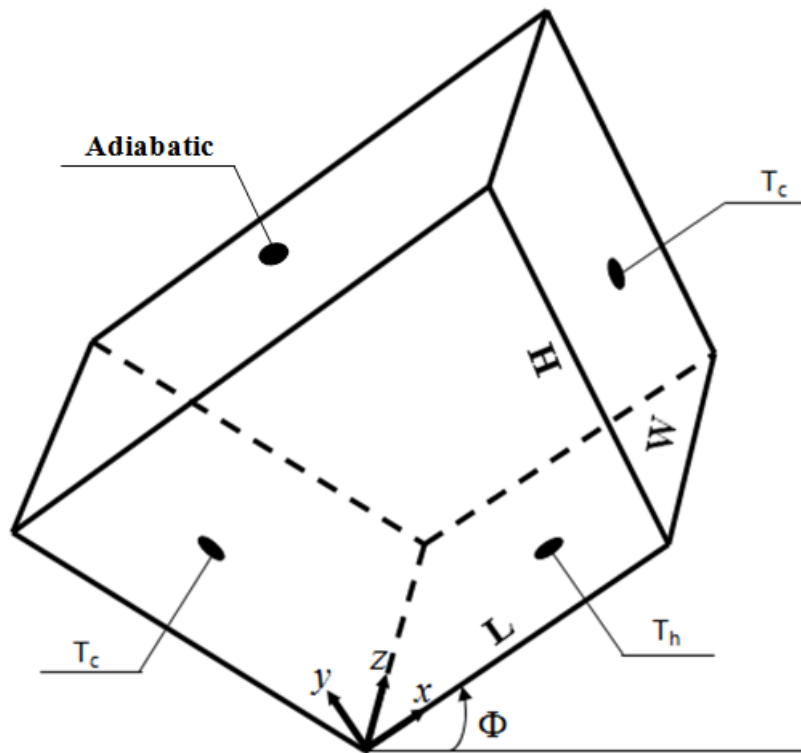


Fig. 1 Schematic diagram of the present problem.

Table 1. Comparison of average Nusselt number at the bottom wall at $Pr = 0.7$, $Da = 10^{-3}$, $Ha = \Delta = 0, \psi = 0^0$.

Ra	Present	Basak et al. [22]
8×10^3	1.952272	1.933142
10^4	2.072541	1.954831

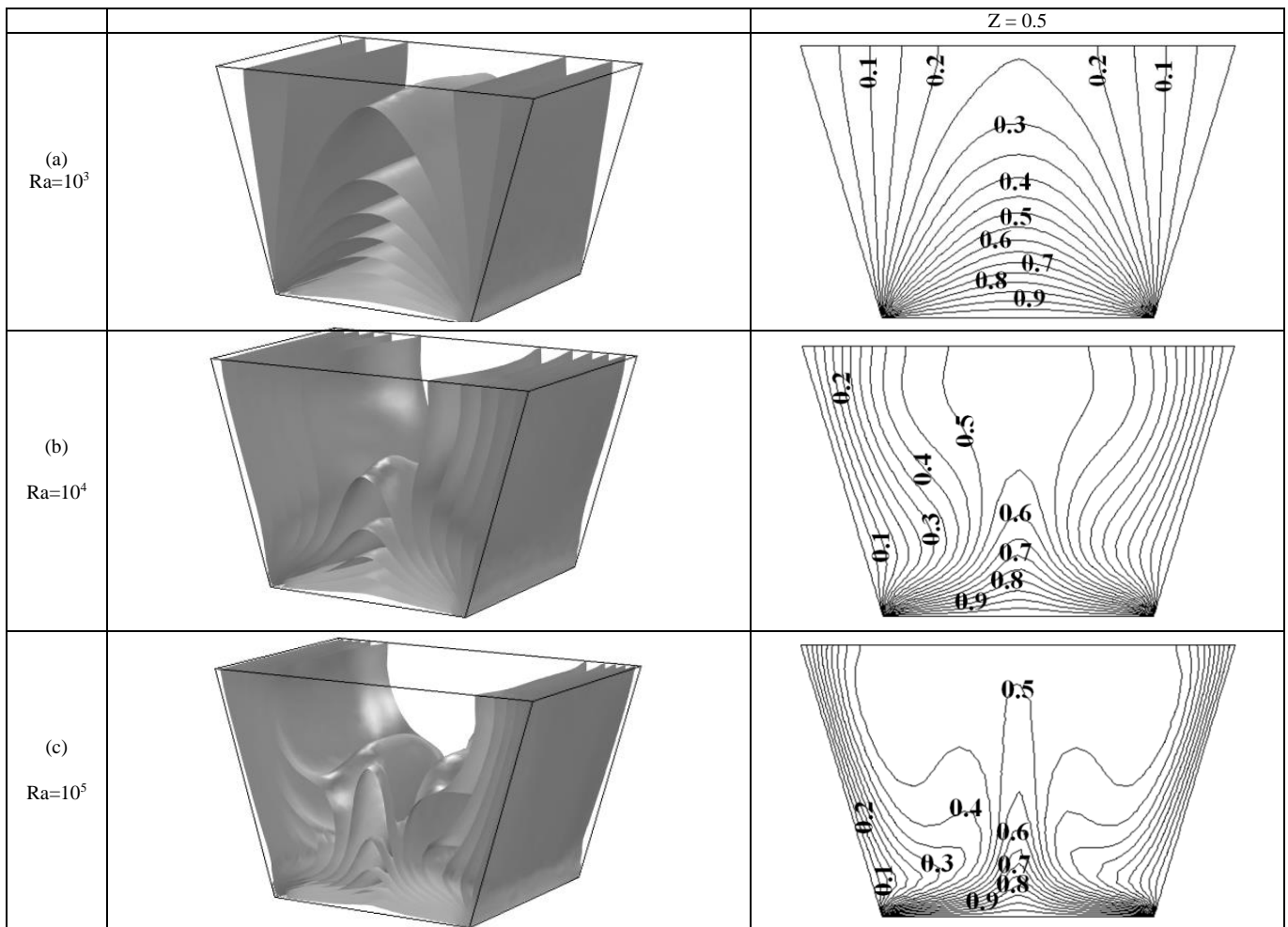


Fig. 2 The isosurfaces of temperature around the all geometry (left) and isotherms along the mid-section (right) in the cubical trapezoidal cavity [$\Phi = 0^\circ$] for various values of Rayleigh number (a) Ra = 10³, (b) Ra = 10⁴ and (c) Ra = 10⁵.

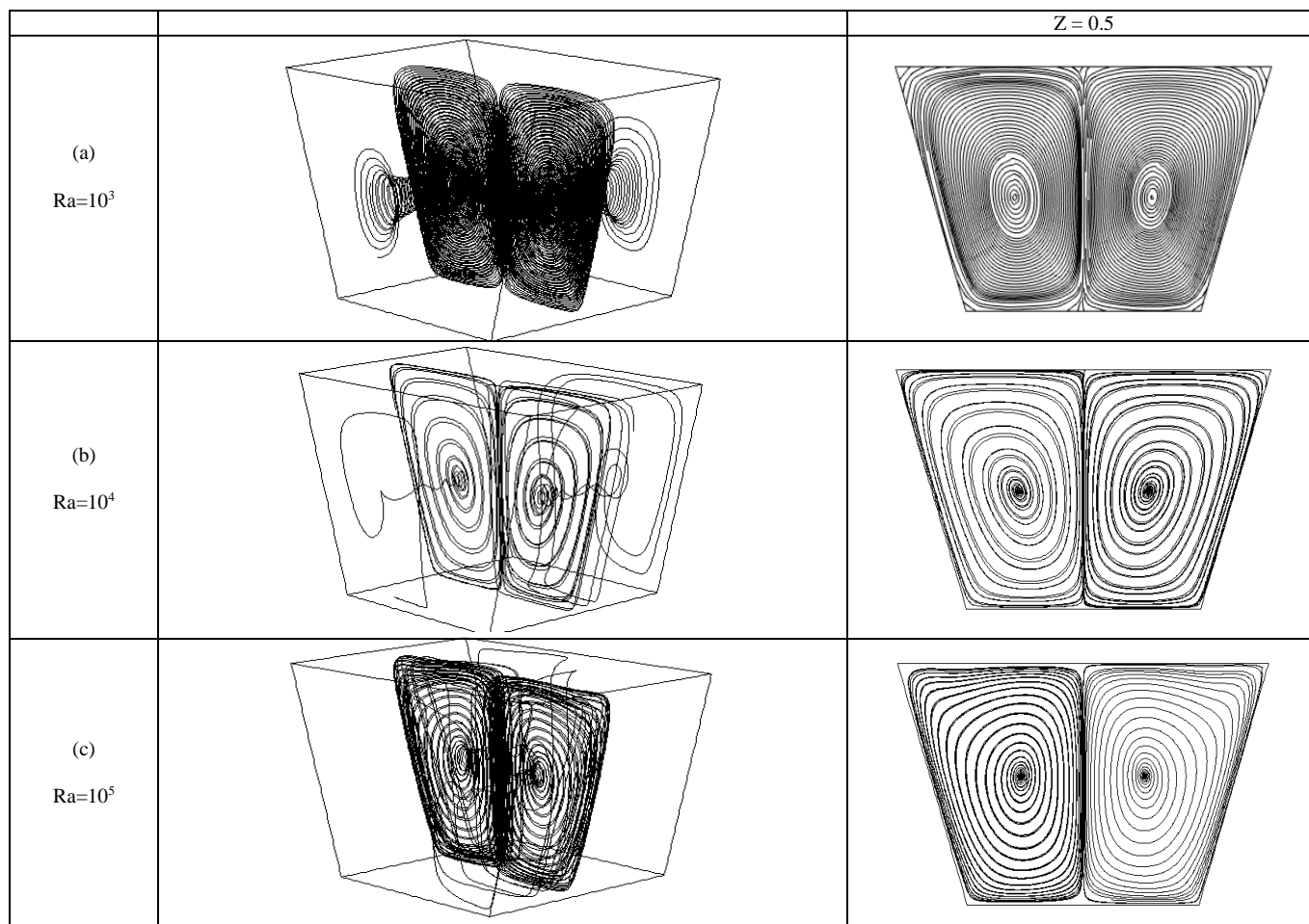


Fig. 3 The trajectory of particles around the all geometry (left) and streamlines along the mid-section (right) in the cubical trapezoidal cavity [$\Phi = 0^\circ$] for various values of Rayleigh number (a) $Ra = 10^3$, (b) $Ra = 10^4$ and (c) $Ra = 10^5$.

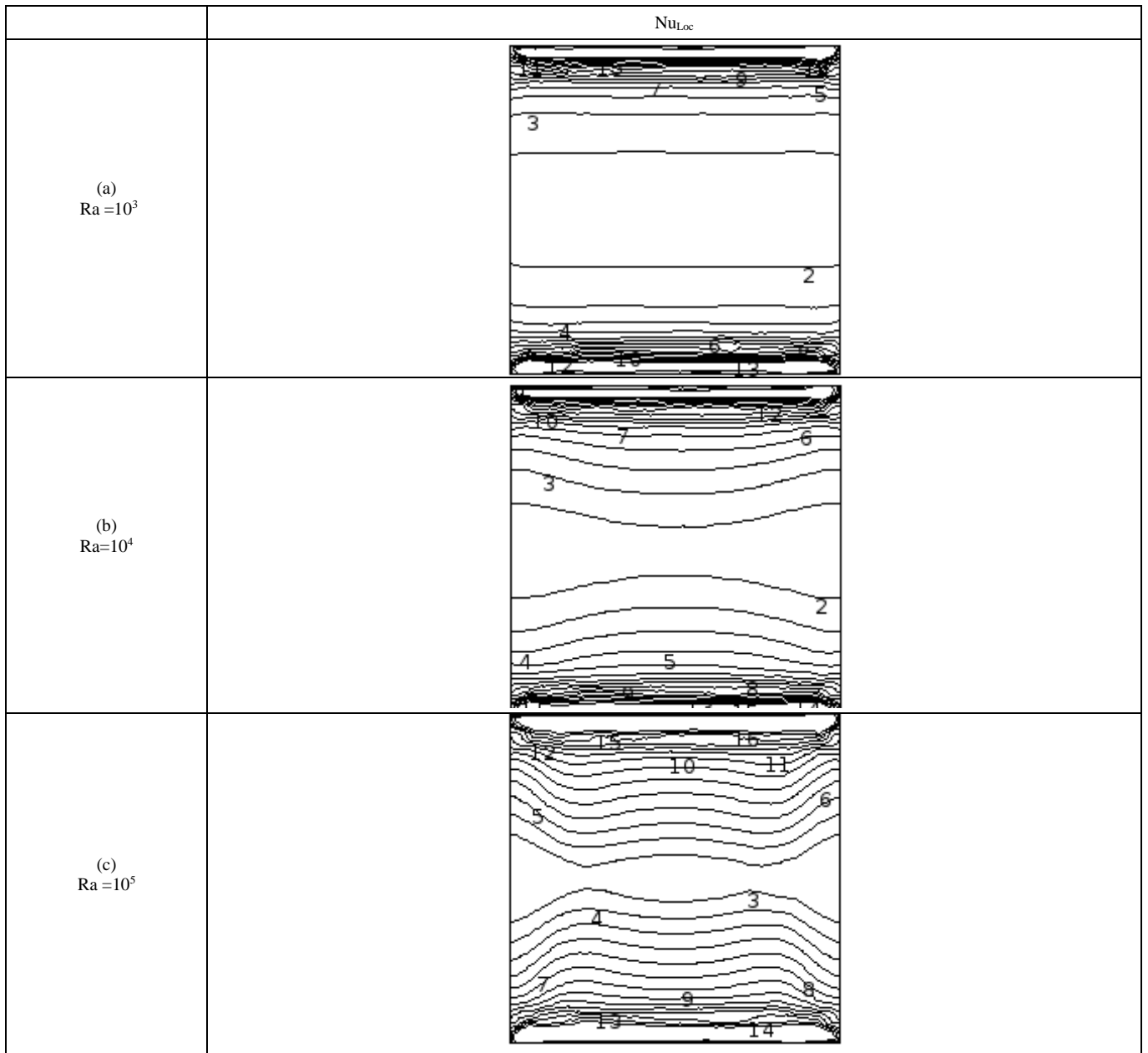


Fig. 4 The variation in the local Nusselt numbers at the hot lower wall in the cubical trapezoidal cavity [$\Phi = 0^\circ$] for various values of Rayleigh number [(a) $Ra = 10^3$, (b) $Ra = 10^4$ and (c) $Ra = 10^5$].

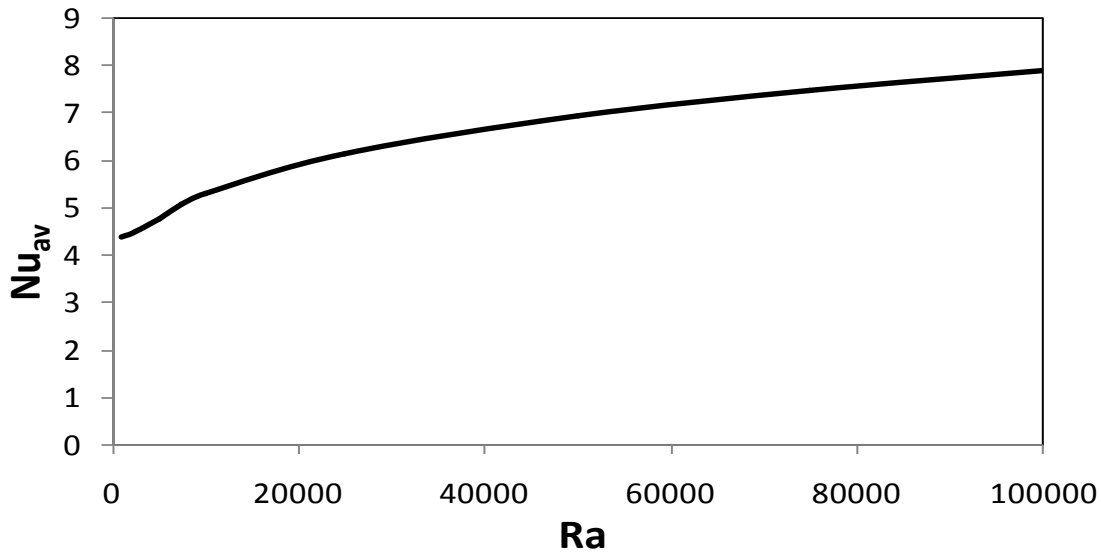


Fig. 5 The variation in the average Nusselt numbers in the cubical trapezoidal cavity [$\Phi = 0^\circ$] for various values of Rayleigh number.

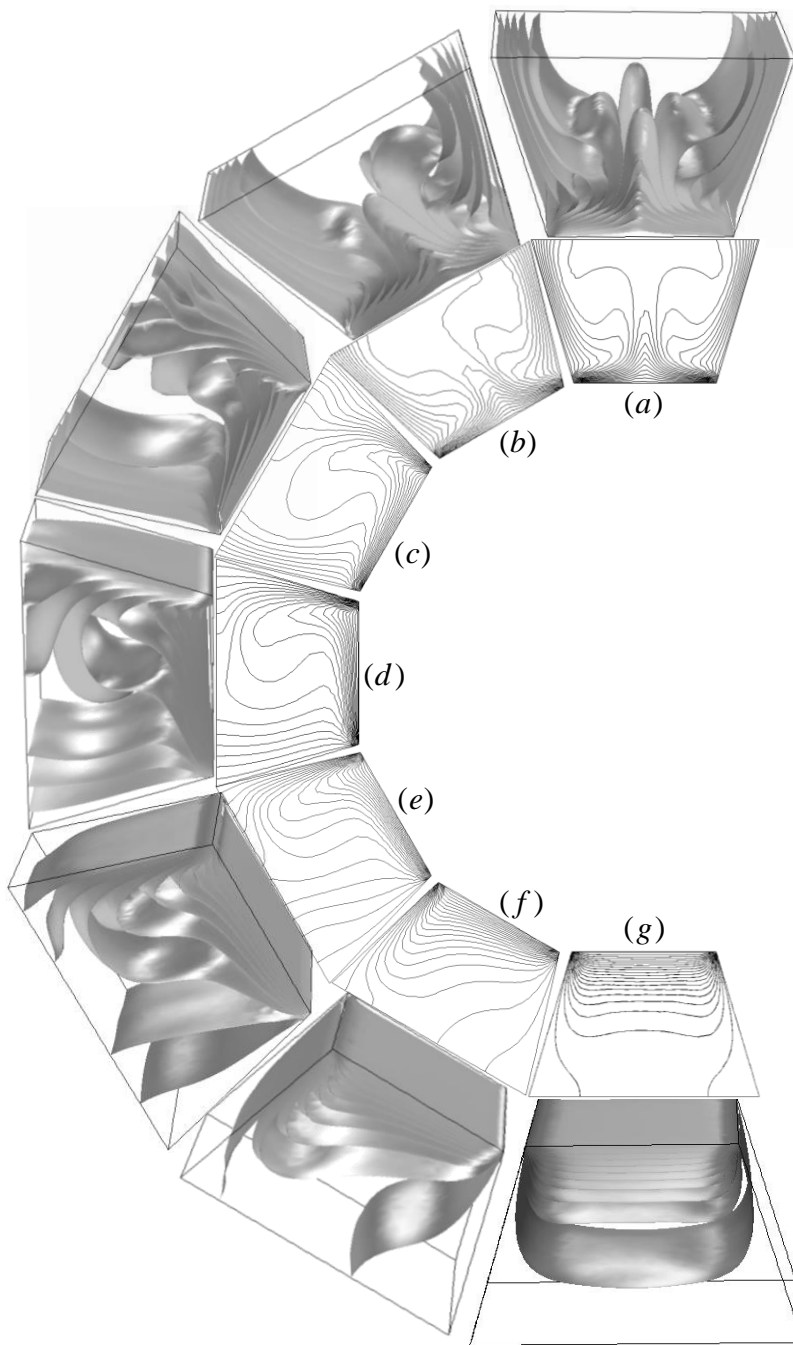


Fig. 6 The isosurfaces of temperature around the all geometry (upper) and isotherms along the mid-section (lower) in the cubical trapezoidal cavity at $[Ra = 10^5]$ and various values of inclination angle [(a) $\Phi = 0^\circ$; (b) $\Phi = 30^\circ$; (c) $\Phi = 60^\circ$; (d) $\Phi = 90^\circ$; (e) $\Phi = 120^\circ$; (f) $\Phi = 150^\circ$ and (g) $\Phi = 180^\circ$].

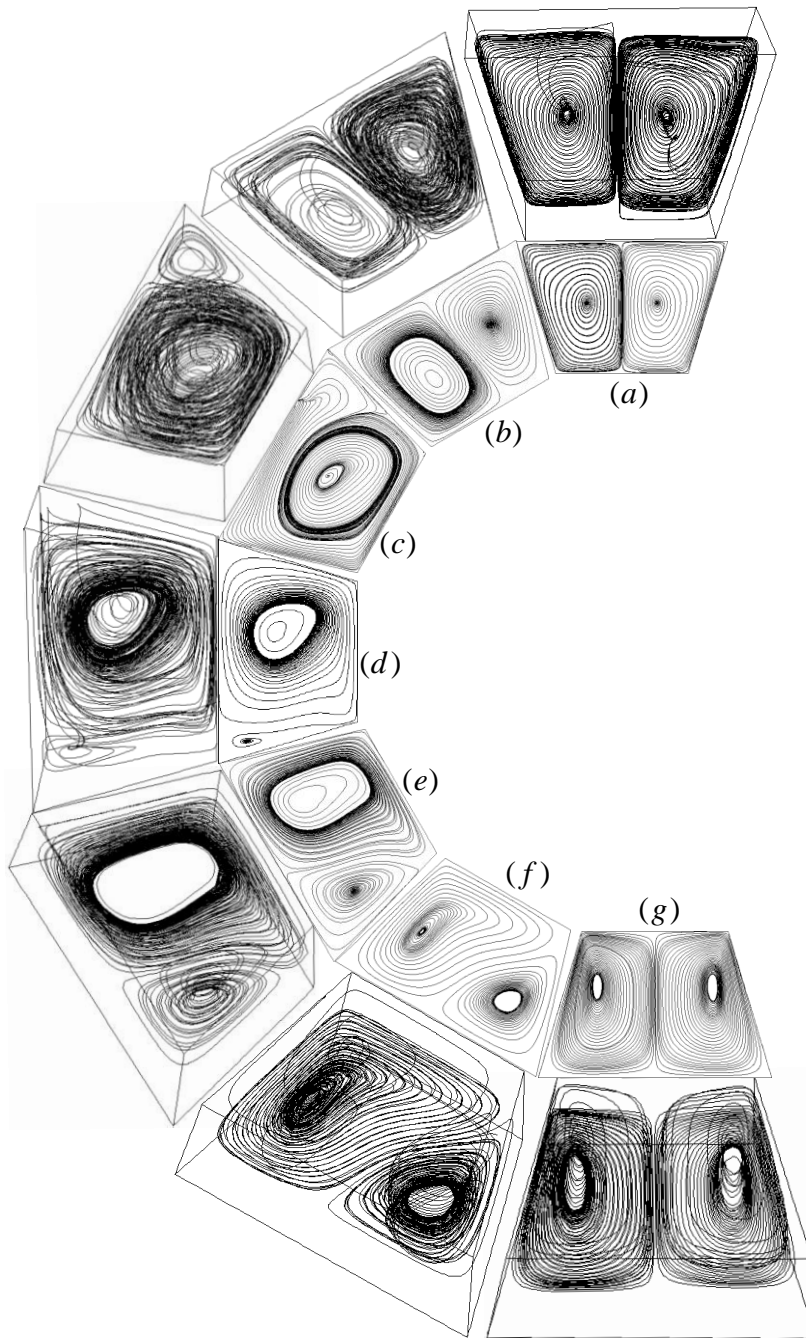


Fig. 7 The trajectory of particles around the all geometry (upper) and streamlines along the mid-section (lower) in the cubical trapezoidal cavity at $[Ra = 10^5]$ and various values of inclination angle [(a) $\Phi = 0^\circ$; (b) $\Phi = 30^\circ$; (c) $\Phi = 60^\circ$; (d) $\Phi = 90^\circ$; (e) $\Phi = 120^\circ$; (f) $\Phi = 150^\circ$ and (g) $\Phi = 180^\circ$].

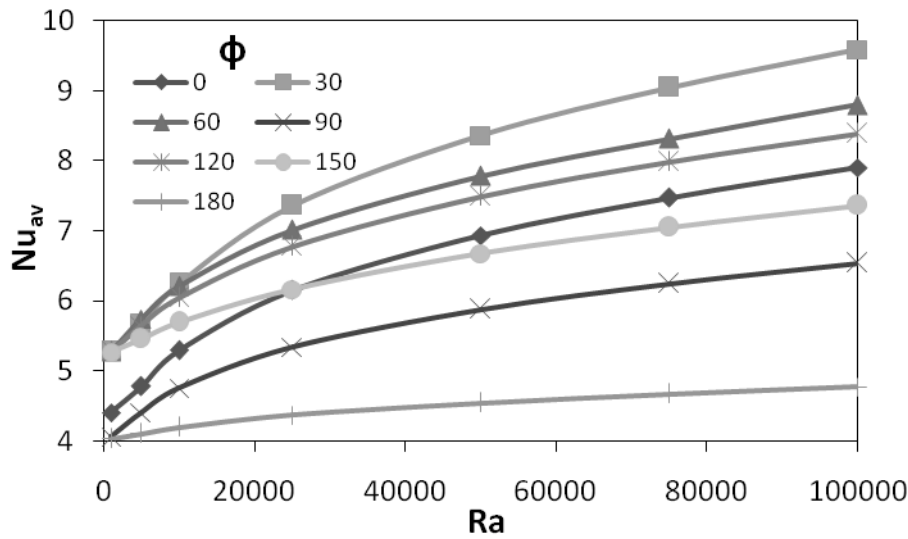


Fig. 8 The relationship between the average Nusselt numbers in the cubical trapezoidal cavity and Rayleigh number for various values of inclination angle.

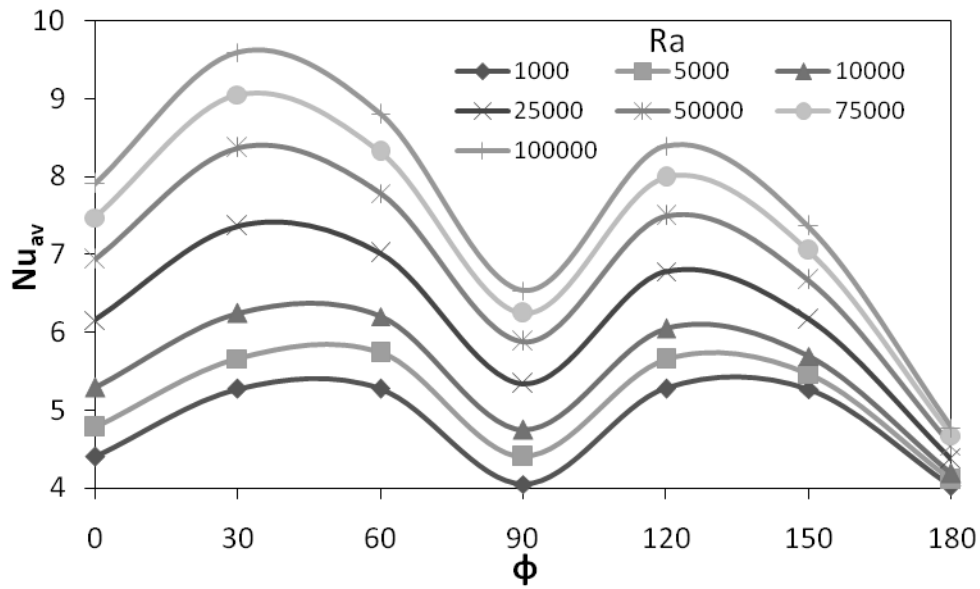


Fig. 9 The relationship between the average Nusselt numbers in the cubical trapezoidal cavity and inclination angle for various values of Rayleigh number.

Nomenclature :		
Symbol	Description	Unit
g	Gravitational acceleration	m/s ²
H	Height of the trapezoidal enclosure	m
k	Fluid thermal conductivity	W / m. °C
n	Unit vector normal to the wall	
L	Length of the trapezoidal enclosure	m
Nu	Nusselt number	
Pr	Prandtl number	
Ra	Rayleigh number	
T	Dimensionless temperature [$(T' - T'_c) / (T'_h - T'_c)$]	
T _o	Bulk temperature [$T_o = (T'_c + T'_h) / 2$]	
t	Dimensionless time ($t' \alpha / L^2$)	
\vec{V}	Dimensionless velocity vector ($\vec{V}' L / \alpha$)	
W	Depth of the trapezoidal enclosure	m
x	Dimensionless Cartesian coordinate in x-direction (x' / L)	
y	Dimensionless Cartesian coordinate in y-direction (y' / H)	
z	Dimensionless Cartesian coordinate in z -direction (z' / L)	
Greek Symbols		
α	Thermal diffusivity	m ² /s
β	Thermal expansion coefficient	K ⁻¹
ΔT	Dimensionless temperature difference	
Φ	Trapezoidal enclosure inclination angle	degree
ν	Fluid kinematic viscosity	m ² /s
$\vec{\psi}$	Dimensionless vector potential ($\vec{\psi}' / \alpha$)	
μ	Dynamic viscosity	kg./m.s
$\vec{\omega}$	Dimensionless vorticity ($\vec{\omega}' \alpha / L^2$)	
Subscripts		
av	Average	
c	Cold	
h	Hot	
Loc	Local	
x, y, z	Cartesian coordinates	
Superscripts		
'	Dimensional variable	